Improvements in Tropical Cyclone Track and Intensity Forecasts Using the GFDL Initialization System

MORRIS A. BENDER, REBECCA J. ROSS, ROBERT E. TULEYA, AND YOSHIO KURIHARA

Geophysical Fluid Dynamics Laboratory, National Oceanic and Atmospheric Administration, Princeton University, Princeton, New Jersey

(Manuscript received 17 July 1992, in final form 23 November 1992)

ABSTRACT

The initialization scheme designed at GFDL to specify a more realistic initial storm structure of tropical cyclones was tested on four real data cases using the GFDL high-resolution multiply nested movable mesh hurricane model. Three of the test cases involved Hurricane Gloria (1985) in the Atlantic basin; the fourth involved Hurricane Gilbert (1988) in the Gulf of Mexico. The initialization scheme produced an initial vortex that was well adapted to the forecast model and was much more realistic in size and intensity than the storm structure obtained from the NMC T80 global analysis. As a result, the erratic storm motion seen in previous integrations of the GFDL model has been nearly eliminated with dramatic improvements in track forecasts during the first 48 h of the prediction. Using the new scheme, the average 24-h and 48-h forecast error for the four test cases was 58 and 94 km, respectively, compared with 143 and 191 km for the noninitialized forecasts starting from the global analysis. The average National Hurricane Center operational forecast error at 24 and 48 h was 118 and 212 km for the same four cases. After 48 h the difference in the average track error became small between the integrations starting from the global analysis and the forecasts starting from the fields obtained by the initialization scheme.

With accurate specification of the initial vortex structure, changes in the storm intensity were also well predicted in these cases. The model correctly forecasted the rapid intensification of Hurricane Gloria just after the system was first upgraded to a hurricane. The model storm intensification also ceased at approximately the same time as observed, with gradual weakening as the storm moved north and approached the east coast of the United States. In the forecast of Hurricane Gilbert, the model storm initially weakened as it moved over the Yucatan Peninsula and underwent only moderate reintensification after moving over the Gulf of Mexico, in good agreement with observations.

Finally, in the case where the track of Hurricane Gloria was well forecast, the distribution of the maximum low-level winds was accurately predicted as the storm moved up the east coast of the United States. During this period the model successfully reproduced many observed features such as large asymmetries in the wind field, with strongest winds occurring well east of the storm center, and a sharp decrease of the wind speed at the coast. Although the asymmetry in the wind distribution was reproduced to a first order in the forecast starting with the global analysis, the agreement with observations was much better with the specified vortex, primarily due to a more realistic radius of maximum wind and storm intensity.

1. Introduction

The purpose of this paper is to demonstrate the improvements in the forecasting of hurricane track, intensity, and structure when the initialization scheme of Kurihara et al. (1993, to be hereafter referred to as KBR) is used to generate tropical cyclones with more realistic structure in the initial conditions of the Geophysical Fluid Dynamics Laboratory (GFDL) high-resolution nested movable mesh hurricane model. Results from four real-data cases are presented in this study. Three of the cases involved predictions of Hurricane Gloria (1985) in the Atlantic basin, while the fourth involved forecasts of Hurricane Gilbert (1988) in the Gulf of Mexico.

In previous forecasts of actual hurricanes using the GFDL high-resolution hurricane model (i.e., Kurihara et al. 1990, hereafter referred to as KBTR), the model successfully simulated many of the observed structural features of Hurricane Gloria as it accelerated to the north and moved up the east coast of the United States. Since the model correctly forecasted the evolution of the large-scale flow during this period, the hurricane track was reasonably well predicted. However, in these experiments the model initial condition was taken from a lower-resolution global analysis in which the hurricane structure was not well resolved. This often resulted in erratic storm motion during the first one or two days of the integration as the vortex underwent a false spinup and adjusted to both the much finer model resolution as well as the differences in physics from the global model. The position error due to this erratic motion during the early period of the forecast equaled or exceeded the errors resulting from inaccuracy in the pre-

Corresponding author address: Morris A. Bender, Geophysical Fluid Dynamics Laboratory, Princeton University, P.O. Box 308, Princeton, NJ 08542-0308.

diction of the steering flow. As a result the position error during the first 24 h, which was strongly affected by this spinup process, was comparable to and, in some cases, worse than the 48-h position error. In addition, since the initial analyzed vortex was usually much too weak, intensity forecasts were impossible starting from this type of vortex structure. It was speculated in KBTR that use of a more realistic vortex in the initial condition would likely reduce the track forecast error from the initial time to 48 h and perhaps beyond. In addition, it was also speculated that forecast skill of storm intensity and structure could become feasible if the initial tropical cyclone was realistic.

The initialization scheme of KBR tries to rectify the shortcomings of the KBTR predictions by producing an initial vortex structure that is more realistic and also well adapted to the hurricane prediction model. In the KBR scheme the original vortex is removed from the analysis and replaced by a new vortex (hereafter referred to as the specified vortex) consisting of both symmetric and asymmetric components. The symmetric component of the specified vortex is generated by the time integration of an axisymmetric version of the hurricane model, ensuring consistency in the vortex structure and compatibility with the physics and resolution of the three dimensional hurricane prediction model. In addition, available observations are used to constrain the axisymmetric vortex development toward a structure representative of the observed storm. An asymmetric wind field is then generated from the symmetric flow by the time integration of a simplified barotropic vorticity equation including the beta effect. Both the symmetric and asymmetric components of the specified vortex are merged back into the modified analysis (excluding the original vortex) at the correct storm position.

The improvements in the forecasting of the storm motion and intensity will be the main focus of the paper. Although numerical models have been employed successfully in operational hurricane track prediction, similar skill has not yet been obtained on a routine basis for the forecast of storm intensity. For each of the four cases presented, track and intensity forecasts will be shown for the integrations with the specified vortex as well as the integrations run with the vortex of the original National Meteorological Center (NMC) global analysis. Comparisons will be made between the two integrations in each set, to determine the impact of the initialization scheme on the prediction of track, intensity, and storm structure.

A brief description of the model, initial conditions, vortex specification, and classification of experiments in this study, will be presented in section 2. In section 3, the predicted storm tracks will be shown for the four sets of integrations. Prediction of the changes in hurricane intensity and storm structure will be shown in section 4. Finally a summary and discussion of the results will be presented in section 5.

TABLE 1. Grid system of the triply nested mesh model used in each experiment.

Mesh	Grid resolution (deg)	Domain size: Latitude (deg)	Latitude (points)	Longitude (deg)	Longitude (points)	Time step (s)
1	1	75	(75)	75	(75)	90
2	1/3	11	(33)	11	(33)	30
3	1/6	5	(30)	5	(30)	15

2. Experimental design

a. Model description

The multiply nested movable mesh (MMM) model described previously by Kurihara and Bender (1980) was used for all the integrations. Specific model details have been outlined in previous publications (e.g., Tuleya et al. 1984; Bender et al. 1987). The model is a primitive equation model formulated in latitude, longitude, and sigma coordinates, with 18 levels in the vertical (i.e., Table 1 of KBTR). The grid system for each of the triply nested meshes in the present study is summarized in Table 1. The outermost domain ranged from 10°S to 65°N in the meridional direction and from either 115° to 40°W (integrations of Hurricane Gloria) or 125° to 50°W (integrations of Hurricane Gilbert). This was 20° larger in both directions than the outer grid used in KBTR, which stretched from 0° to 55°N and 95° to 40°W. The model physics include a cumulus parameterization described by Kurihara (1973), with some modification [Kurihara and Bender (1980), appendix C], a Monin–Obukhov scheme for the surface flux calculation, and the Mellor and Yamada (1974) level 2 turbulence closure scheme for the vertical diffusion, with a background diffusion coefficient added. There are several modifications to the model since KBTR. Specifically, in the formulation for the surface flux calculations, the roughness length z_0 and the evaporation efficiency W over land are now a function of the specific vegetation type of that particular region on the globe (see appendix A for more details). Over the ocean, where z_0 is determined by Charnock's relation (e.g., Kurihara and Tuleya 1974), the Charnock constant of 0.032 has been modified to an updated value of 0.0185 (Wu 1982). Finally, the three-point smoothing that has been used in previous versions of the model has now been modified to include a desmoothing operator as well (see appendix B).

b. Model initial condition and experimental design

As in KBTR, the initial data were obtained from the NMC T80 global analysis and were horizontally interpolated onto the regional model domain for each of the mesh resolutions. The distribution of surface

height was obtained from the global topography dataset prepared by the U.S. Navy's Fleet Numerical Oceanography Center at Monterey, California. The temperature, surface pressure, and moisture fields over land were then adjusted for the differences between the NMC and the navy topographical heights. The sea surface temperatures were set equal to the NMC analyzed values at the start of the integration and held fixed throughout each experiment.

The integrations presented in this study were run from four initial times. To assess the impact of the initialization scheme on the model forecasts, two separate integrations were performed starting from each of these times. The first integration of each set began from an initial condition containing the original vortex resolved by the global analysis. The second began from the initial condition modified by the new initialization scheme.

Each of the model predictions was run in forecast mode (e.g., Orlanski and Katzfey 1987) with the data taken at 12-h intervals from an integration of the T80 spectral model. In all of the experiments the specified lateral boundary values were linearly interpolated in time to hourly values, and the model solution was then forced toward the next future hourly values at every time step using the lateral boundary forcing scheme of Kurihara et al. (1989).

TABLE 3. Data sources used to determine the specified vortex for the four experiments.

Data source	Distance of observations used (km) from storm center
Gloria (0000 UTC 22 September 1985)	
HRD aircraft at 500 hPa	125 (radius of maximum winds)
HRD aircraft at 500 hPa	200, 300
Gloria (0000 UTC 24 September 1985)	
HRD aircraft at 500 hPa	30 (radius of maximum winds)
HRD aircraft at 500 hPa	60, 140, 300
Gloria (0000 UTC 25 September 1985)	
HRD aircraft at 400 hPa	30 (radius of maximum winds)
HRD aircraft at 400 hPa	40, 90
Marine advisories	115 (radius of 64-kt winds)
Marine advisories	162 (radius of 50-kt winds)
Surface wind observations	325, 400
Gilbert (1200 UTC 22 September 1988)	
HRD aircraft at 700 hPa	30 (radius of maximum winds)
HRD aircraft at 700 hPa	70, 120, 150
Marine advisories	235 (radius 50-kt winds)
Surface wind observations	600, 700

c. *Vortex specification*

As described by KBR two kinds of filters were used in the first step of the initialization process to remove the original vortex from the large-scale analysis. The new specified vortex, consisting of both symmetric and asymmetric components, was merged with the nonhurricane component of the analysis at the correct position of the observed storm as determined from the National Hurricane Center best-track position. The size of the new specified vortex, r_b, was based on available observations and, thus, is distinct from the radius r_0 that defines the region of the analysis containing the original vortex. The values of r_0 and r_b are listed in Table 2 for each of the four experiments. The experiments discussed here preceded the implementation of the automated system described in section 6 of KBR. Comparison of Table 2 with Table 1 of KBR shows the changes in these values that resulted from the automated system. Another difference was the value of the cylindrical filter parameter l [Eq. (3.8), KBR]. For the integrations presented here it was set to $0.5r_0$, while in KBR it was $0.2r_0$. Also shown in Table 2 are the initial position errors of the original analyzed vortices from the observed storm positions. Because the original vortex position error can sometimes exceed 100 km, positioning the specified vortex to the observed NHC best-track position was important.

TABLE 2. The values of r_o, r_b and the initial position error for the four cases presented in this study.

Storm (initial time)	r_o (km)	r_b (km)	Initial position error (km)
Gloria (1200 UTC 22 September 1985)	1050	745	130
Gloria (0000 UTC 24 September 1985)	1050	805	110
Gloria (0000 UTC 25 September 1985)	1050	960	20
Gilbert (1200 UTC 14 September 1988)	1450	1350	30

As outlined in KBR, the symmetric component of the specified vortex was generated by the time integration of an axisymmetric version of the MMM hurricane model. During the axisymmetric integration, the tangential wind field was forced toward an estimate of the observed storm tangential wind profile, while the moisture, mass, and radial wind profiles were free to develop a model-consistent structure. The data sources used to determine the profile of the tangential wind are summarized in Table 3 for each of the experiments. Near the storm center, the primary data source used was the aircraft flight-level wind plots provided by Hurricane Research Division, Atlantic Oceanographic and Meteorological Laboratory. Parameters related to storm size such as the radius of hurricane-force winds and the radius of 50-kt winds were obtained from the National Hurricane Center's marine advisories. The

profile of the storm's tangential wind in the outer radii was estimated from any available low-level wind observations. It should be pointed out that the initialization technique has been formulated to determine the best estimate of the radial profile of the tangential wind using whatever data are available at the time of initialization.

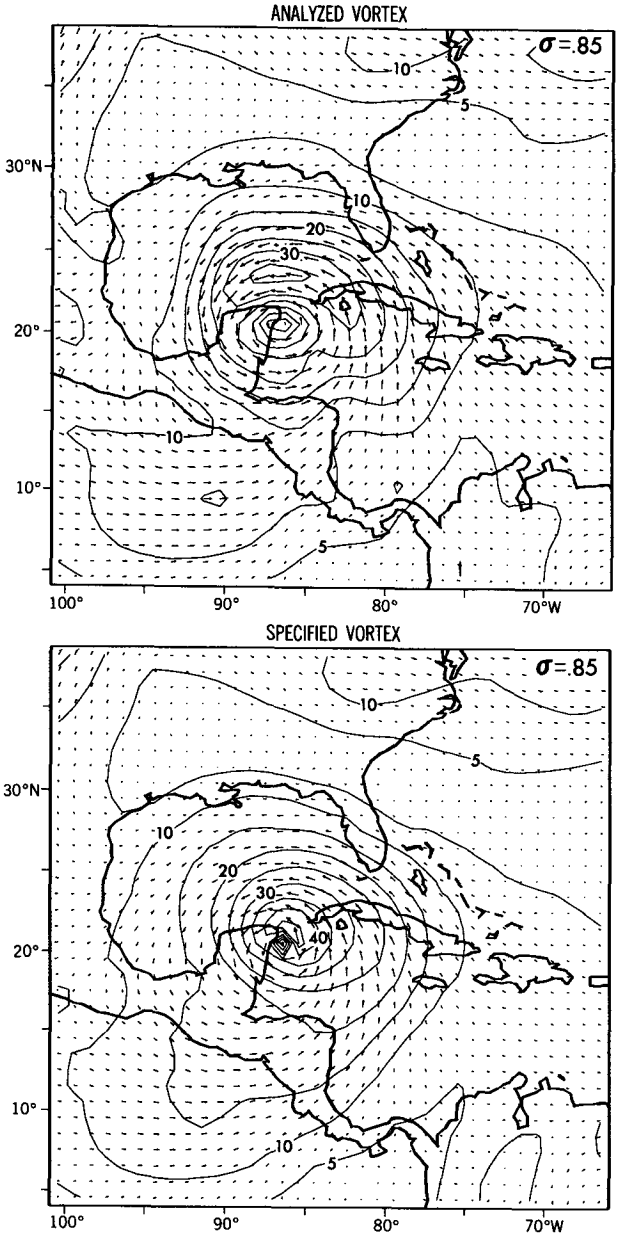

FIG. 1. Distribution of horizontal wind vectors and wind speed (m s^{-1}) at 1200 UTC 14 September 1988 (Hurricane Gilbert) at model level 14 (σ = 0.856), for both the global analysis (top) and the specified vortex (bottom). The region shown is for a portion of the integration domain surrounding the storm region. The wind distribution shown, plotted with a 5 m s^{-1} contour interval, is for the wind field resolved by the 1° resolution.

Since a significant component of tropical cyclone motion can result from its asymmetric structure (e.g., Carr and Elsberry 1990; Smith et al. 1990), the symmetric flow generated from the previous step was used to generate an asymmetric wind field. This was accomplished by the time integration of a simplified barotropic vorticity equation with the beta effect included (Ross and Kurihara 1992), which ensured that the asymmetric and symmetric components were mutually consistent. The sum of the symmetric and asymmetric components yielded the specified vortex that was subsequently merged back into the large-scale analysis in which the analyzed vortex was excluded. Finally, the new mass field was recomputed from the divergence equation with its time tendency appropriately controlled. Initialization of the mass field ensured a reasonably smooth start of the integration of the prediction model. The improvement in the structure of the specified vortex is readily apparent in Fig. 1. Here, the wind distributions are presented (model level 14, σ = 0.856) for both the original NMC global analysis and the initial condition with the specified vortex, for one of the set of experiments used in this study (i.e., Hurricane Gilbert, 1200 UTC 14 September 1988). The specified vortex is much more compact and considerably more intense than the vortex in the global analysis, with the radius of maximum wind decreasing from 350 km to about 60 km.

d. Classification of experiments

The nine integrations presented in this study are listed in Table 4. The number in each experiment name refers to the starting date of the experiment. The letter N at the end of the integration name refers to those forecasts integrated with the vortex resolved by the NMC global analysis. Likewise, those forecasts integrated with the specified vortex are designated by the letter S. The first six integrations listed in Table 4 refer to predictions of Hurricane Gloria. The last three refer to integrations of Hurricane Gilbert. The last experiment listed (G14-NA) refers to a supplemental experiment where the symmetric part of the specified vortex was retained, but the initial asymmetries were removed. The results from G22N and G25N differed from the results shown for G22F and G25F in KBTR primarily due to the increase in the size of the outermost domain as well as the improvements in the model physics outlined in section 2a.

3. Hurricane track prediction

The previous forecasts of Hurricane Gloria described in KBTR demonstrated considerable skill in track prediction, which was attributed primarily to the successful simulation of the large-scale environmental flow. However, one of the primary sources of track error was the adjustment of the initial vortex to the model physics and resolution. The focus of this section is to report

TABLE 4. Summary of numerical experiments discussed.

Experiment name	Initial time	Type of vortex used
G22N	1200 UTC 22 September 1985	Analyzed vortex
G22S	1200 UTC 22 September 1985	Specified vortex
G24N	0000 UTC 24 September 1985	Analyzed vortex
G24S	0000 UTC 24 September 1985	Specified vortex
G25N	0000 UTC 25 September 1985	Analyzed vortex
G25S	0000 UTC 25 September 1985	Specified vortex
G14N	1200 UTC 14 September 1988	Analyzed vortex
G14S	1200 UTC 14 September 1988	Specified vortex
G14-NA	1200 UTC 14 September 1988	Specified vortex

the improvement in track forecast that has resulted from the use of the specified vortex compared to the original analyzed vortex. In this section storm tracks will be shown for the four sets of integrations performed in this study. Three of the cases involved Hurricane Gloria (1985) in the Atlantic basin, and the fourth involved Hurricane Gilbert (1988) in the Gulf of Mexico.

a. Hurricane Gloria (1200 UTC 22 September 1985)

For the first set of integrations the initial field was obtained from the T80 analysis on 1200 UTC 22 September, 18 h after Gloria was first upgraded from a tropical storm to a hurricane (Fig. 2). The observed hurricane recurved to the north after four days and accelerated to the north-northeast 12 h later. Thus, this first case began well before the time of recurvature of the system. In previous integrations by KBTR with the analyzed vortex, the two primary sources of track error were the erratic and too rapid movement of the storm during the first two days of the forecast as well as premature recurvature of the model storm that occurred about 24 h too soon.

The model was integrated for 132 h starting from both initial vortices (G22N and G22S). A significant improvement in the forecasted track resulted in the use of the specified vortex (G22S) during the early period of the forecast (Fig. 3). The smoothness of the track in G22S during the first 24 h, in comparison with the erratic storm track in G22N during the same period, indicates that the initial adjustment of the vortex in G22N has been nearly eliminated by the initialization scheme. The 24-h forecast error decreased from 119 to about 56 km. By 48 h the improvement was even larger. In the integration with the analyzed vortex (G22N), rapid movement of the storm resulted in a 48-h forecast error of 458 km. With the specified vortex, the storm motion was still too fast, but the 48-h position error was reduced to 206 km. By 72 h the storm in G22N was located about 300 km west-southwest of the storm in G22S. After 72 h both storms began to prematurely recurve to the north, moving well east of the observed storm track (Fig. 4). By the end of the integration (132 h) the forecast errors for G22N and G22S were 646 and 670 km, respectively. These large position errors were partly the result of excessive storm acceleration between 96 and 120 h as well as the premature recurvature of the model storm. Thus, the primary improvements in the forecasted storm position attributable to the initialization scheme were limited to the

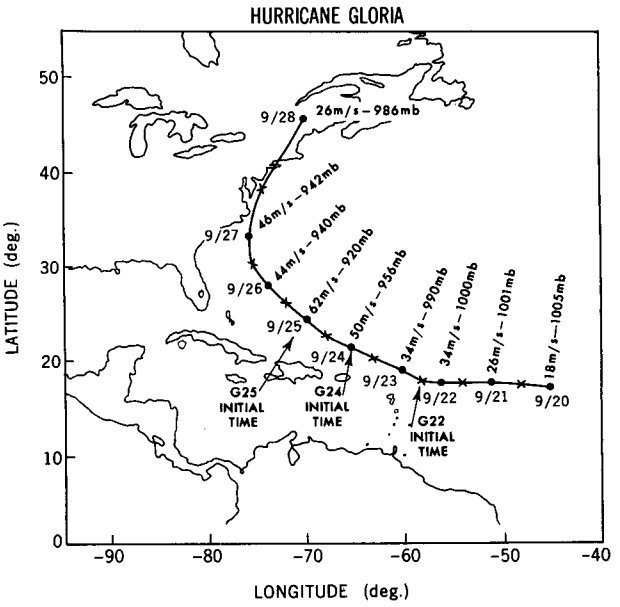

FIG. 2. Observed track (best track determined by the National Hurricane Center) of Hurricane Gloria during the period from 0000 UTC 20 September 1985 until 0000 UTC 28 September 1985. The storm's minimum sea level pressure (mb) and maximum low-level wind (m s^{-1}) at 0000 UTC each day are shown. The large dots indicate the position of the storm at 0000 UTC and the X's indicate the 1200 UTC storm positions. The initial starting times for the three sets of Hurricane Gloria forecasts are also indicated.

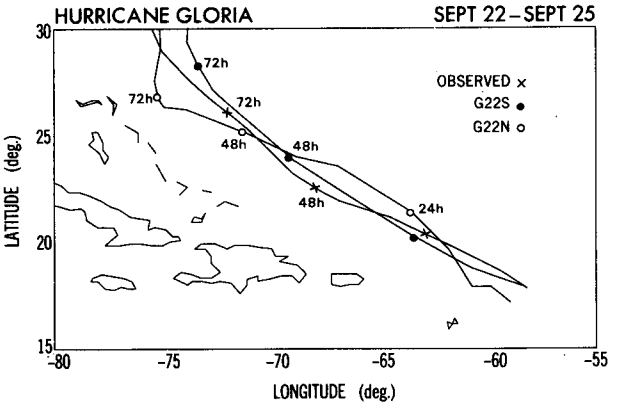

FIG. 3. An enlarged portion of the storm tracks from forecasts G22S and G22N (1200 UTC 22 September 1985 starting time) plotted at 6-h intervals. For comparison, the observed track (best track) is also plotted. The symbols indicate the daily storm positions valid at 1200 UTC each day.

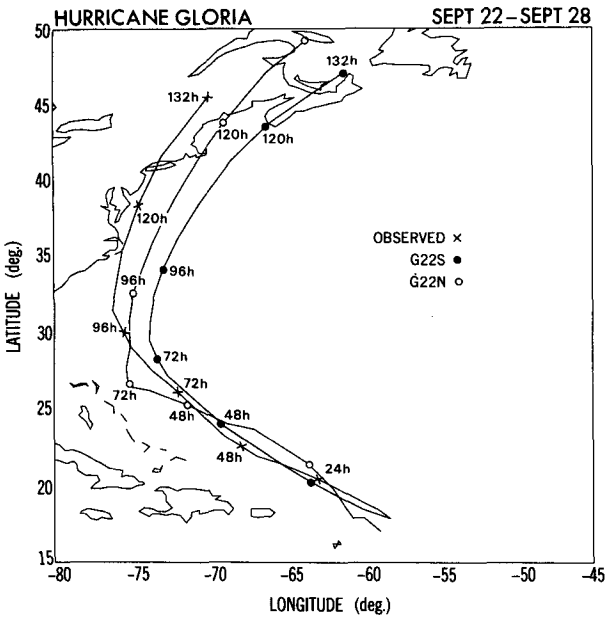

FIG. 4. The storm tracks from forecasts G22S and G22N for the entire 132-h period. The best track is also plotted. Daily storm positions (valid at 1200 UTC each day), as well as the final storm position, are indicated by the symbols.

first 72 h of the integration. Use of the specified vortex also resulted in a significant reduction in the track error compared to the NHC official forecast issued near the start of the forecast period that exhibited errors of 212, 336, and 514 km at 24, 48, and 72 h compared to 56, 206, and 274 km for G22S.

In order to isolate the cause of the errors affecting the storm tracks after 72 h, the streamlines and isotachs of the deep-layer mean wind (defined by KBTR in section 3) were computed (Fig. 5) for the T80 analysis and G22S at 1200 UTC 25 September (hour 72 of the forecast). As noted in KBTR, the storm motion for Hurricane Gloria seemed to closely parallel the streamlines of the deep-layer mean wind field obtained by this technique. In Fig. 5, the orientation of the anticyclone to the east of the storm was southeast to northwest in the T80 analysis, in contrast to a south–north orientation of this feature forecasted by the model. As a result, the mean flow in the vicinity of the storm in the analysis was basically southeasterly, in good agreement with the observed storm direction at that time. In contrast, the mean flow forecasted by the model was southerly in this region, which began to steer the model storm toward the north and resulted in recurvature of the storm at that time. A similar feature existed in the large-scale flow field predicted by the T80 forecast model (figure not shown). Therefore, the premature recurvature of both predicted storms was clearly a consequence of inaccuracies in the forecasted evolution of the large-scale flow.

b. Hurricane Gloria (0000 UTC 24 September 1985)

In the next set of integrations the initial field was obtained from the T80 analysis on 0000 UTC 24 September during the period in which Gloria was undergoing rapid intensification (Fig. 2), and about 60 h before the system recurved. The model was integrated to 96 h for this set of integrations. As shown in Fig. 6,

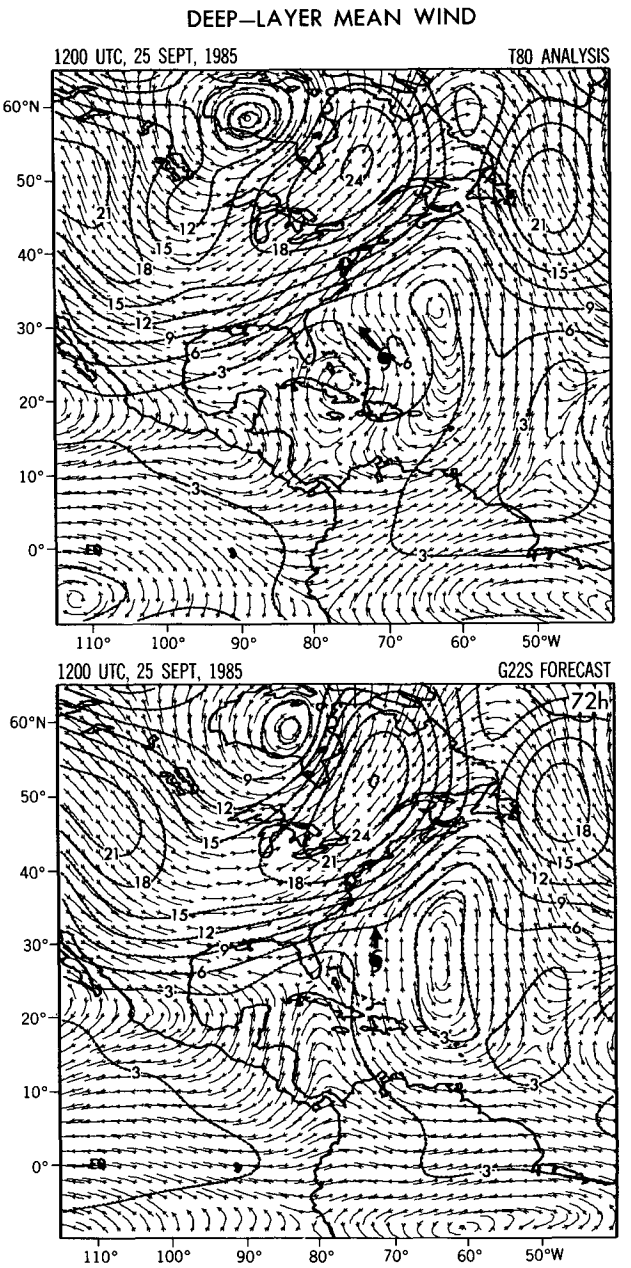

FIG. 5. The streamlines and isotachs (thick dashed line) of the deep-layer mean wind at 1200 UTC 25 September 1985 for the T80 analysis (top) and G22S (bottom). The region shown is for the entire integration domain used for the experiment. The observed (top) and forecasted (bottom) 72-h storm position is indicated by the hurricane symbol, with the storm direction of motion shown by the thick arrow.

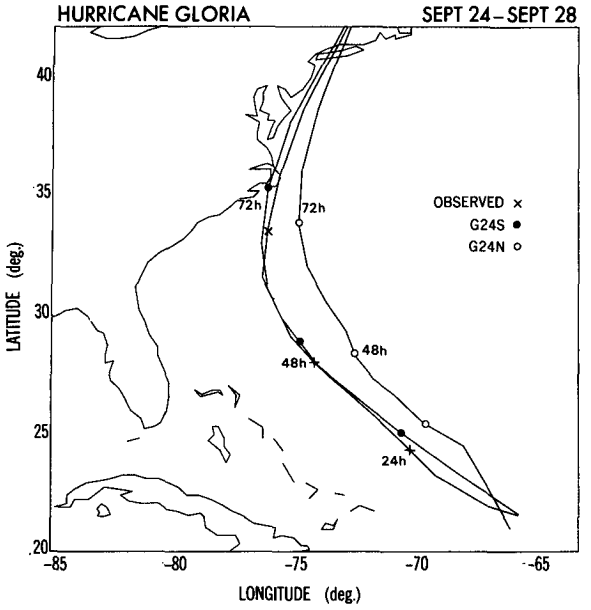

FIG. 6. A portion of the storm tracks from forecasts G24S and G24N (0000 UTC 24 September 1985 starting time). For comparison, the observed track (best track) is also plotted. The symbols indicate the daily storm positions valid at 0000 UTC each day.

the G24N vortex moved in basically a northwest to north-northwest direction during the first 18 h of the forecast, in contrast to an observed west-northwest motion. This resulted in a 24-h position error of 137 km. Analysis of the G24N model fields during this period indicated that a region of large convergence and heavy precipitation formed north of the storm, as the unrealistically large vortex (with radius of maximum winds of over 450 km compared to a 30-km observed value) adjusted to the fine resolution of the model. This resulted in a more northerly direction of motion as the vortex continued its spinup process, and the radius of maximum wind decreased in size. By 24 h the radius of maximum wind had decreased to about 170 km.

In contrast, the specified vortex did not undergo significant adjustment initially and, thus, the storm moved in the observed west-northwest direction from the initial time. Thus, the 24-h forecast error was reduced to about 85 km. Similar to experiment G22S, most of the forecast error associated with the specified vortex resulted from too rapid movement of the storm. However, the recurvature of the system was correctly forecasted for both G24S and G24N. The 48-h and 72-h forecast error for G24S was 118 and 221 km, respectively, compared to 173 and 132 km for G24N. Throughout the entire integration, the track forecast for G24S remained remarkably good, with the model storm making landfall over Long Island approximately 15 km to the west of the observed landfall position but about 6 h too early. For all three time periods, use of the specified vortex yielded reductions in the track error compared to the NHC official forecast that produced position errors of 102, 198, and 398 km, respectively.

c. Hurricane Gloria (0000 UTC 25 September 1985)

In the third set of integrations the initial field was obtained from the T80 analysis on 0000 UTC 25 September, when Hurricane Gloria had reached its mature stage with maximum intensity of 920 mb (Fig. 2). The storm tracks of the two 72-h integrations are shown in Fig. 7. Once again, use of the specified vortex resulted in significant improvements in the track prediction during the first two days of the integration. The erratic movement of the storm in G25N was eliminated in G25S resulting in a 24-h and 48-h forecast error for G25S of 47 and 30 km, compared to 189 and 58 km for G25N. It is interesting to note that despite the dramatic improvements in the track forecast during the early part of the forecast, the 72-h positions were very similar as both G25S and G25N failed to forecast the proper amount of recurvature of the storm after 48 h. Since the system was accelerating at this time, very small errors in the large-scale flow field resulted in large errors in the storm position. The 72-h forecast errors for G25S and G25N were 259 and 226 km, respectively, which still showed considerable improvement compared to the position error of 480 km from the NHC official forecast. Likewise, the position error of 92 and 165 km in the NHC forecast at 24 and 48 h was also considerably reduced in G25S.

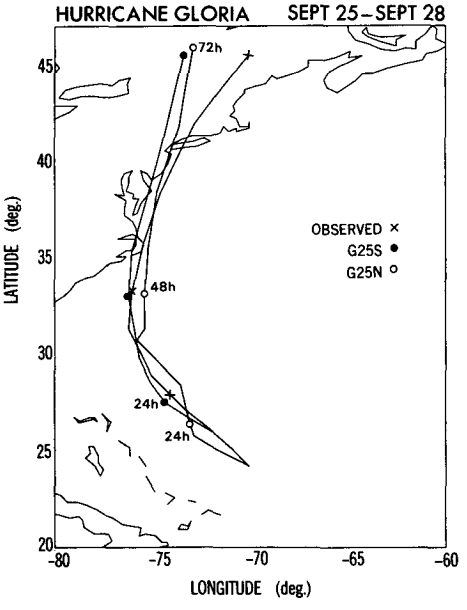

FIG. 7. The storm tracks from forecasts G25S and G25N (0000 UTC 25 September 1985 starting time). For comparison, the observed track (best track) is also plotted. The symbols indicate the daily storm positions valid at 0000 UTC each day.

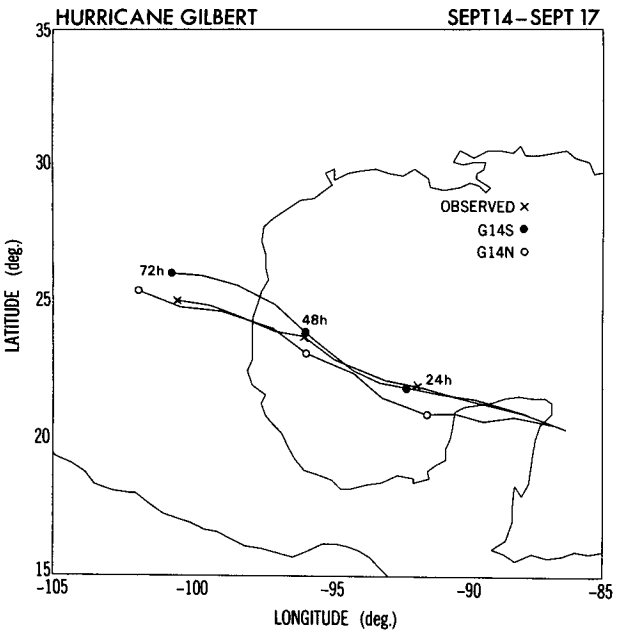

FIG. 8. The storm tracks from forecasts G14S and G14N (1200 UTC 14 September 1988 starting time). For comparison, the observed track (best track) is also plotted. The symbols indicate the daily storm positions valid at 1200 UTC each day.

d. Hurricane Gilbert (1200 UTC 14 September 1988)

In the last set of integrations that involved 72-h forecasts of Hurricane Gilbert, the initial field was obtained from the T80 analysis at 1200 UTC 14 September 1988, just prior to the landfall of the hurricane on the Yucatan Peninsula. At that time the hurricane was near maximum intensity with a minimum sea level pressure of 892 mb and maximum low-level winds of about 72 m s^{-1}. In contrast to Hurricane Gloria, Gilbert remained at low latitudes throughout its entire history and was also characterized by a very large circulation (r_b = 1350 km).

The storm tracks for the two integrations are shown in Fig. 8. Once again, significant improvement in the track forecast occurred during the first 48 h of the forecast with the specified vortex (G14S). Without the specified vortex (G14N), the vortex moved erratically for the first 24 h. The 24- and 48-h positions of G14N were 125 km southwest and 73 km south of the best-track position. In contrast, the storm track with the specified vortex (G14S) remained very close to the best track during the first 48 h of the forecast, with a 24- and 48-h forecast error of only 44 and 22 km. Between 48 and 60 h the storm in G14S began to move slightly more to the north compared to the best-track position. This resulted in a forecast error of 109 km at 72 h compared with a 150-km forecast error for G14N. In contrast, the 24-h, 48-h, and 72-h position error of the NHC forecast issued near the start of the forecast period was 64, 150, and 654 km, respectively. Since the NHC predicted storm track turned sharply to the north-northwest during the third day, a large forecast error resulted.

In order to understand the evolution of the synoptic situation during the forecast period, the environmental conditions that existed during this period were examined. The deep-layer mean wind field was computed from the global analysis, both at the initial time (Fig. 9, top) and 48 h later (Fig. 9, bottom). At the initial time, the hurricane was embedded in a large-scale wave in the easterlies, with an anticyclone over Florida located to the northeast of the storm center. During the next 48 h the anticyclone over Florida began to build to the southwest, with southeasterly winds gradually spreading into the Gulf of Mexico just behind the storm, as Hurricane Gilbert continued to move in a westward direction. Thus, the precise timing of the storm motion as well as an accurate forecast of the large-scale flow were essential for the accurate prediction of the storm motion in the MMM model, especially during the final day of the forecast. This rapid change in the large-scale flow field, and small errors in the prediction of the southerly flow in the storm region, may have contributed to the large forecast errors in the NHC official forecast after 48 h and their incorrect recurvature of the storm to the north during this time.

Since the circulation of Hurricane Gilbert was very large, the specified vortex included a large asymmetric component (i.e., the asymmetric wind speed maximum was over 5 m s^{-1} at the top of the boundary layer near the storm center). The large asymmetries may have played an important role in the observed direction of motion of Hurricane Gilbert, which remained quite constant throughout this period. A supplemental experiment (G14-NA) was run using the same initial symmetric vortex structure as G14S, but with the asymmetric component removed in order to test the sensitivity of the forecasted track to the initial asymmetries. As seen in Fig. 10, this resulted in a very large change in the forecast track. The storm motion was considerably slower, with the 24-h position of the storm about 85 km to the east of the best-track position and about 180 km east of the best-track position by 48 h. After 24 h the storm began to turn more to the northwest, resulting in a 72-h forecast error of 403 km. It is speculated that this northward movement of the storm may have been partly due to small changes in the environmental flow that occurred with removal of the asymmetries. An additional factor may have been the slower movement of the storm, which caused the southeasterly flow (i.e., Fig. 9, bottom) that was spreading into the Gulf of Mexico to reach the storm area at an earlier time.

For the three cases involving Hurricane Gloria, the maximum asymmetric wind component near the storm center was 1.2 m s^{-1} for G22S (1200 UTC 22 September 1985), 2.1 m s^{-1} for G24S (0000 UTC 24

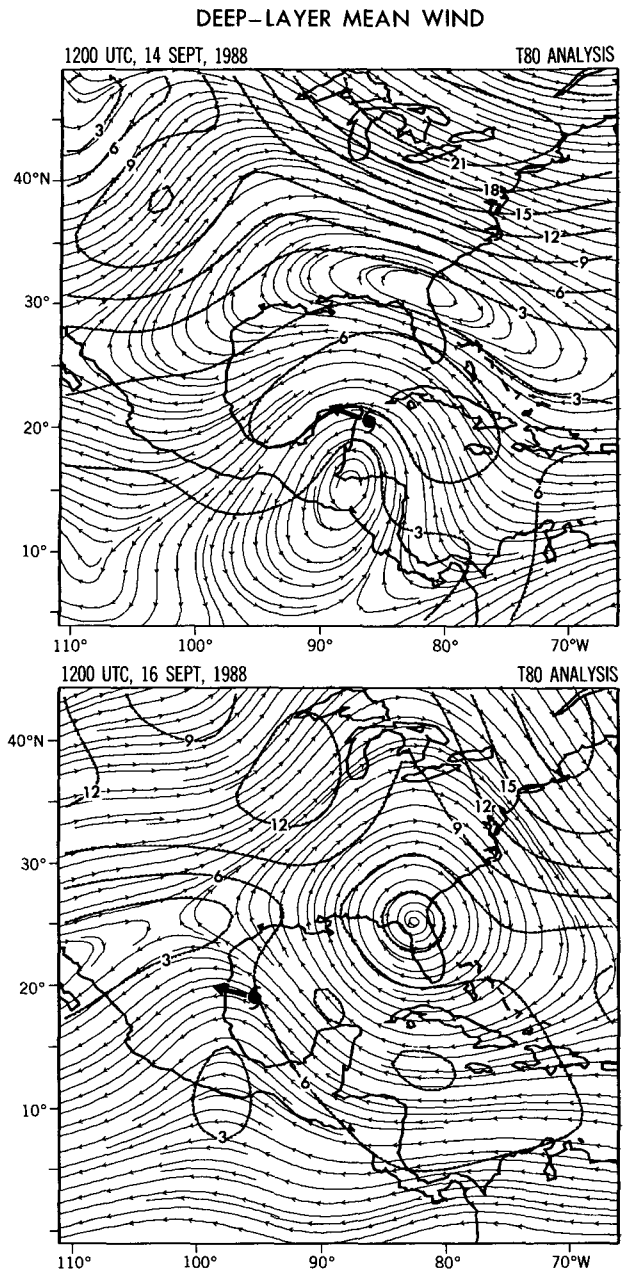

FIG. 9. The streamlines and isotachs (thick line) of the deep-layer mean wind of the T80 analysis at 1200 UTC 14 September 1988 (top) and 1200 UTC 16 September 1988 (bottom). The region shown is a portion of the integration domain used for the forecasts of Hurricane Gilbert. The observed storm position is indicated by the hurricane symbol, with the storm direction of motion shown by the thick arrow.

September 1985), and 3.2 m s^{-1} for G25S (0000 UTC 25 September 1985). For these three cases, removal of the asymmetric component had a much smaller influence on the storm track, although it caused a reduction in the storm speed in each case. This resulted in a small decrease in the position error in G22S and G24S, which were moving too fast, and an increase in the position error for G25S. For example, the 48-h forecast error for these three integrations without asymmetries changed from 206 to 158 km, 118 to 60 km, and finally 30 to 68 km, respectively. Since the storm's movement depends on both the vortex drift due to the asymmetry and the time-dependent large-scale environment, the effect of the asymmetries on the storm track will probably vary from case to case, although the effect should be more important when the large-scale flow is weak or when the storm circulation becomes very large, as in the case of Hurricane Gilbert.

4. Prediction of changes in hurricane intensity and storm structure

The purpose of this section is to demonstrate that with accurate specification of the initial vortex structure, the forecast skill of the GFDL hurricane model was successfully extended to include changes in storm intensity and structure. Each of the three forecasts involving Hurricane Gloria began during separate phases of the hurricane's history (i.e., before the onset of rapid intensification, during the period of rapid intensification, and at the beginning of the mature stage). Also, the forecast of Hurricane Gilbert began just prior to landfall over the Yucatan Peninsula. Thus, each of the four cases addressed a unique aspect of hurricane intensity forecasting. Time series (at 1-h intervals) of minimum sea level pressure and maximum low-level winds determined from the lowest model level (σ

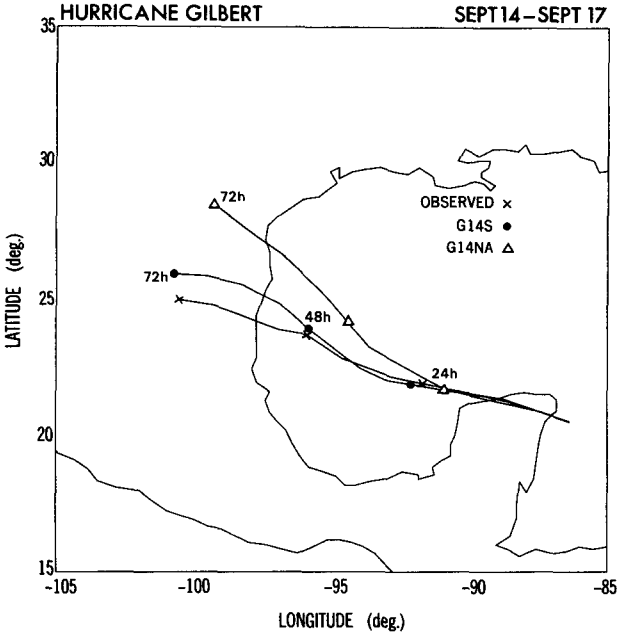

FIG. 10. The storm tracks for forecast G14S and G14-NA, the supplemental forecast including the symmetric vortex but with no asymmetric component initially. See Fig. 8 for more details.

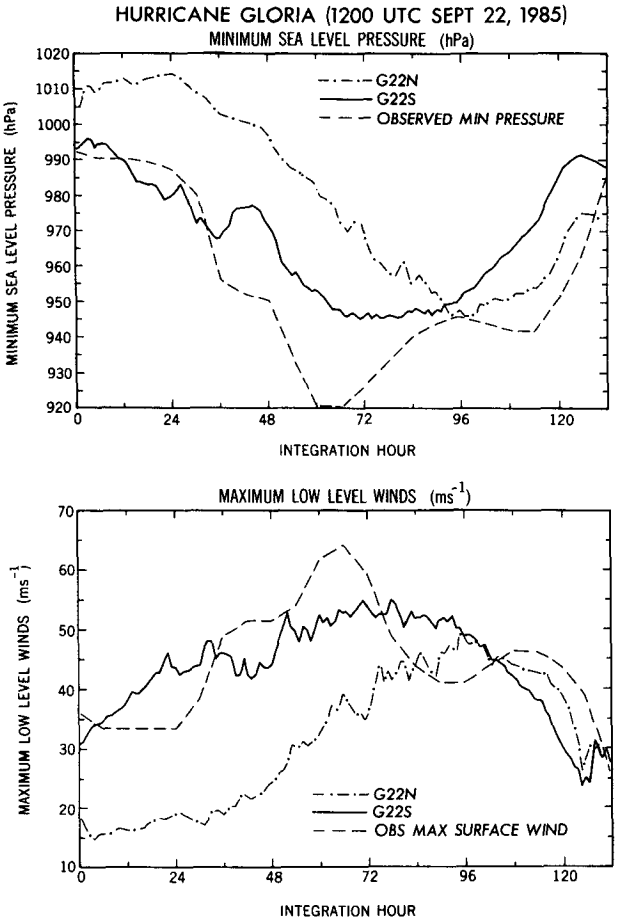

FIG. 11. Time series of minimum sea level pressure (hPa, top) and maximum low-level winds (m s^{-1}, bottom, $\sigma = 0.995$) plotted at 1-h intervals for forecasts G22S and G22N starting at 1200 UTC 22 September 1985. For comparison, the observed minimum sea level pressure and maximum surface wind at 6-h intervals are also plotted.

= 0.995, approximately the 50-m height) will be shown for the integrations presented in this study and compared with the observed values (at 6-h intervals). For one of the cases (G24S), changes in the storm structure that occurred during the forecast will also be shown.

a. Hurricane Gloria (1200 UTC 22 September 1985)

The first set of integrations, G22S and G22N, presented in Fig. 11, began before the onset of rapid intensification of Hurricane Gloria, near the period when the system was first upgraded to a hurricane. During the next 60 h the observed system deepened 72 mb, reaching a maximum intensity of 920 mb around 0000 UTC 25 September (Fig. 2). From Fig. 11 it can be seen that G22S succeeded in correctly forecasting the rapid intensification of the storm during this time, with the model storm deepening nearly 50 mb. It is also interesting to note that intensification ceased at approximately the same time as observed, with gradual weakening thereafter. Although G22N also predicted a similar amount of deepening, the onset of intensification was delayed approximately 24 h, and the period of intensification continued well beyond that of the observed storm. The maximum low-level winds in G22S (Fig. 11b) also show a gradual weakening during the final 3.5 days of the forecast as the storm moved toward the United States coastline (e.g., Figs. 2 and 4) and turned north. The difference between the observed and model intensity during the mature stage may have been due in part to the resolution of the model, which was unable to resolve the very fine structure of the eyewall region. Indeed, the actual radius of maximum wind at the time of maximum intensity (e.g., 0000 UTC September 25) was about 18 km [Fig. 5 of Franklin et al. (1988)] compared to about a 17-km resolution of the inner model grid. The 48-h and 72-h maximum surface winds predicted in G22S were about 45 and 55 m s^{-1} compared to observed values of 51 and 59 m s^{-1} and maximum surface winds of 41 and 46 m s^{-1} forecasted by the NHC. Thus, for G22S the model intensity forecast exhibited significant improvement compared to the NHC forecast during these two time periods.

It is interesting to note that between 36 and 48 h, as the observed storm system was moving north of Puerto Rico (see Fig. 3), the very rapid rate of intensification of the observed hurricane decreased. The storm in G22S also temporarily weakened during this period. Analysis of the moisture fields from G22S indicated that drier air originating from the mountains of Puerto Rico was advected into the storm circulation during this time. Integrations from previous idealized experiments (e.g., Bender et al. 1987) have shown that this can have a significant impact on changes in the storm intensity.

b. Hurricane Gloria (0000 UTC 24 September 1985)

The time series for G24S and G24N presented in this section represent integrations that began during the period in which Gloria was undergoing rapid intensification. An important issue addressed in this set of experiments was whether the model storm would continue to rapidly deepen from the start of the integration without first undergoing a period of adjustment. In addition, since G24S succeeded in accurately forecasting the storm track for the entire forecast period, the distribution of predicted maximum low-level winds was compared with available observations. Successful prediction of this quantity is also dependent on the accurate prediction of changes in both the storm structure and intensity.

As seen in Fig. 12, the storm in G24S began to intensify from the beginning of the forecast, although it could not reproduce the very rapid deepening between 12 and 24 h. We again speculate that this may have

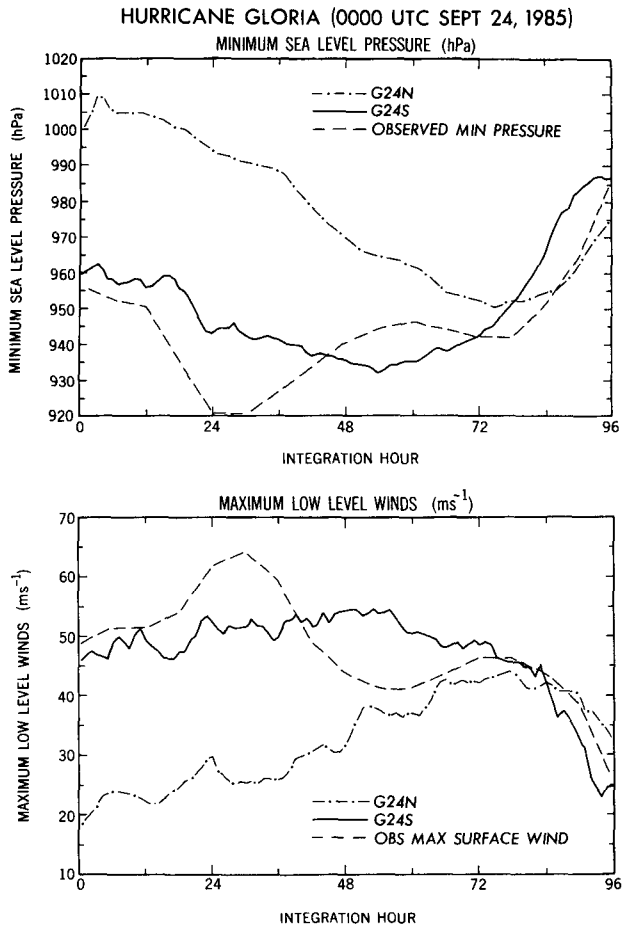

FIG. 12. Same as Fig. 11 but for forecasts G24S and G24N for the 96-h period starting at 0000 UTC 24 September 1985.

been partly due to the resolution of the model. Also, the storm intensification continued beyond 48 h, about 30 h after the observed system. As a result, the forecasted maximum low-level winds were too strong in G24S between 36 and 72 h, resulting in maximum surface winds of about 54 and 49 m s^{-1} at 48 and 72 h compared to observed values of 44 and 46 m s^{-1}. The NHC advisories issued near the start of the forecast period also failed to predict the extent of intensification of the storm as well as the decrease of the winds after 36 h, with forecasted values of 57 m s^{-1} for the maximum surface winds during both time periods. Thus, G24S demonstrated improvement in the forecasted storm intensity compared to the official NHC forecast. In G24N the storm gradually intensified during the first 72 h of the forecast until the storm began to weaken as it approached the United States and moved north over colder waters (Fig. 6).

During this period the storm in G24S underwent changes in the storm structure as well as intensity. For example, during the final 36 h of the forecast the wind field gradually broadened. The radius of maximum wind measured at model level 14 ($\sigma = 0.856$) increased from 60 km at 0000 UTC 25 September to about 90 km 48 h later (Fig. 13) and over 150 km as the storm made landfall over Long Island. Also, as the storm approached the east coast of North Carolina, the strongest winds occurred on the east side of the storm, over the ocean. Thus, during passage of the storm up the East Coast, the model produced strongest winds east of the storm center (Fig. 14). The asymmetry in the wind

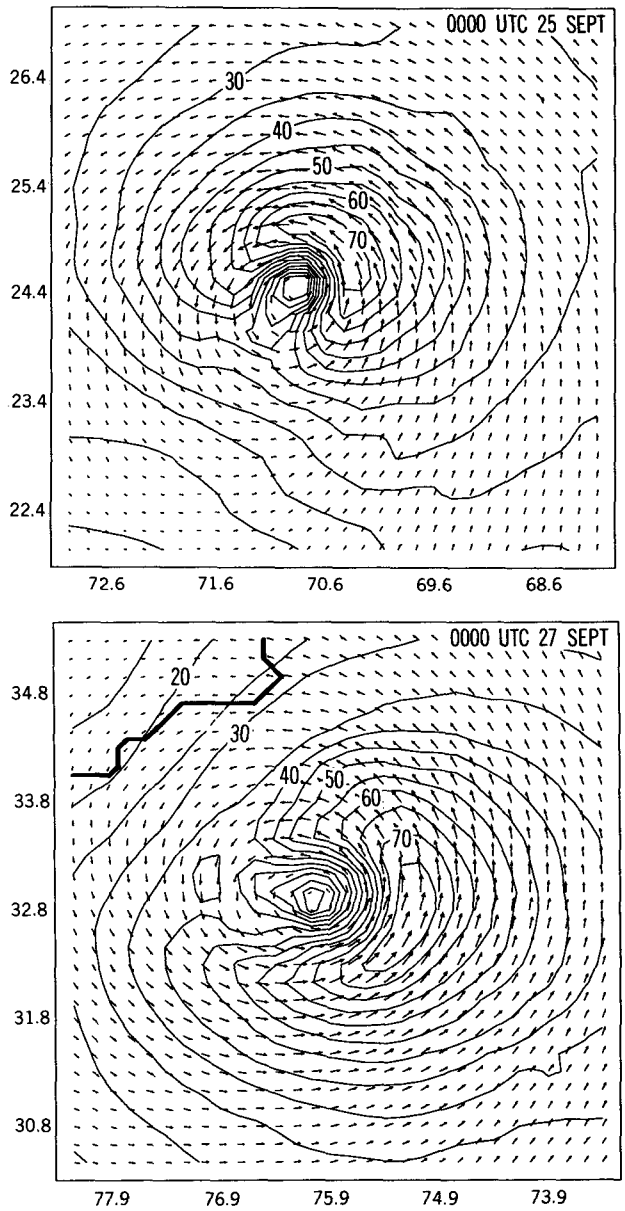

FIG. 13. Distribution of horizontal wind vectors and wind speed (m s^{-1}) at model level 14 ($\sigma = 0.856$) at 24 h (0000 UTC September 25) and 72 h (0000 UTC September 27) of the forecast for G24S. The region shown is the inner mesh (1/6° resolution), with the wind vectors plotted at the resolution of the finest grid. The coastline is indicated by the thick, solid line.

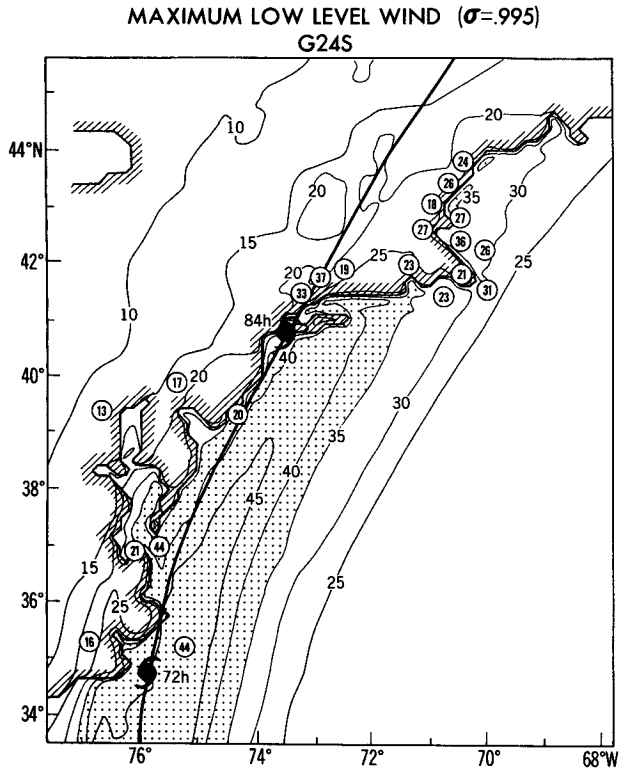

FIG. 14. Distribution of the predicted maximum low-level (σ = 0.995) wind (m s^{-1}) during the passage of Hurricane Gloria, for forecast G24S. Solid lines indicate the wind speeds at 5 m s^{-1} intervals, with areas above 30 m s^{-1} shaded. The numbers in circles are the observed values (m s^{-1}) of the maximum sustained surface winds. The forecasted storm track of the surface pressure center is shown by a thick solid line, with the storm position plotted at 6-h intervals and indicated by a hurricane symbol. Finally, the heavy solid line, with short hatches, indicates the shoreline resolved by the finest mesh resolution (1/6°).

distribution is similar to the results produced by G24N and KBTR (see Fig. 4 of KBTR), although the G24S radius of maximum wind is much more realistic. Also, since the storm system was not undergoing a "spinup" process as it was moving up the coast, the maximum winds gradually decreased as the storm continued moving north. Thus, the agreement with observations improved with G24S. Hurricane-force winds were correctly forecasted along the North Carolina coast, while the strongest winds remained just east of the coast of New Jersey. Similar to the distribution from KBTR, an abrupt decrease of winds occurred across the coastline. Strong winds were also observed well east of the storm center over a large section of the Massachusetts coastline and northward, where wind speeds in excess of hurricane force were observed (Case 1986).

c. *Hurricane Gloria (0000 UTC 25 September 1985)*

The time series for integrations G25S and G25N, which began at the time of Hurricane Gloria's maximum intensity, are presented in Fig. 15. Since these forecasts started at the beginning of the hurricane's mature phase, we examined whether the model could maintain the storm intensity from the beginning of the forecast. Although the storm in G25S underwent some weakening during the first 6 h of the experiment, the storm intensity remained fairly constant until the storm system approached the North Carolina coast at approximately 54 h (Fig. 7). Between 12 and 36 h, G25S failed to forecast the gradual weakening that occurred after Gloria reached its mature stage. However, after 24 h the winds in G25S exhibited a small and gradual decrease throughout much of this period until rapidly decreasing toward the end of the experiment. The 48- and 72-h maximum low-level winds in G25S were 52 and 30 m s^{-1} compared with observed surface winds of 46 and 26 m s^{-1}. The 48- and 72-h maximum surface winds predicted by the NHC advisories issued near the start of the forecast period were 57 and 26 m s^{-1}. Thus, G25S produced an improved intensity forecast at only 48 h compared to the NHC official forecast.

The initial weakening of the storm in G25S is likely the result of the very compact vortex structure that was barely resolvable by the model's finest resolution. In

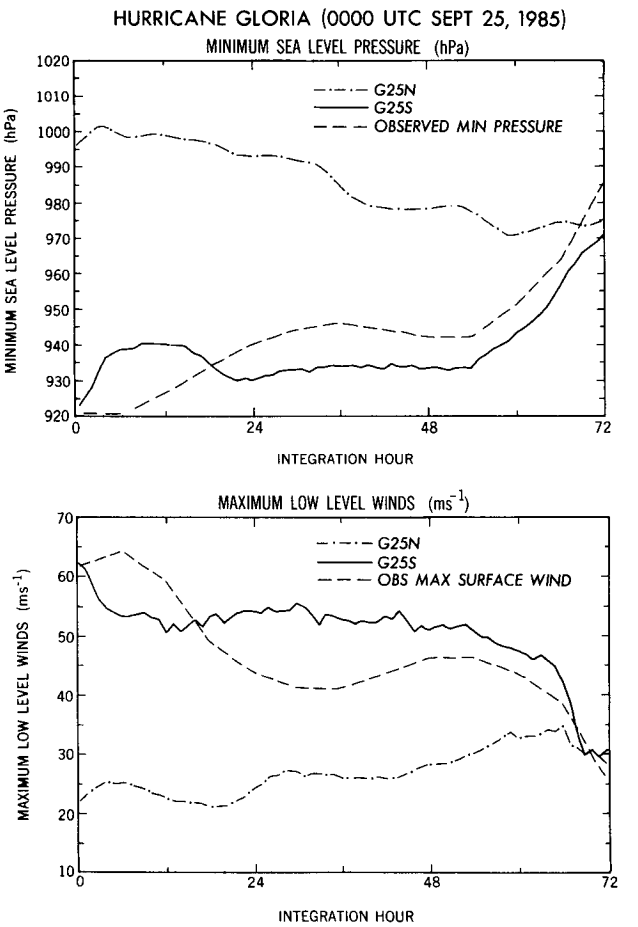

FIG. 15. Same as Fig. 11 but for forecasts G25S and G25N for the 72-h period starting at 0000 UTC 25 September 1985.

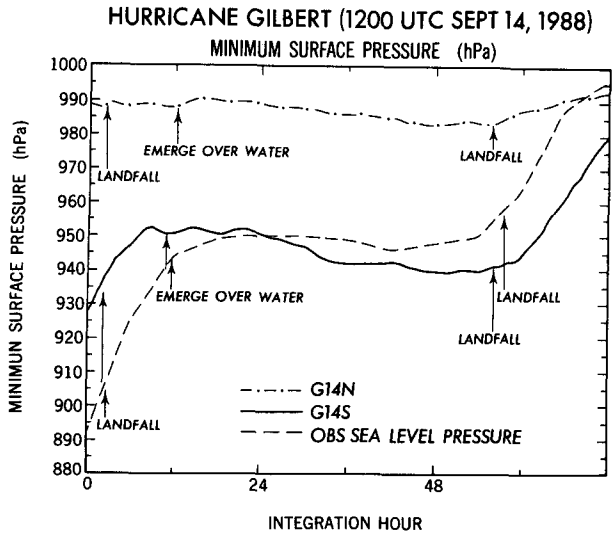

FIG. 16. Time series of minimum sea level pressure (hPa) plotted at 1-h intervals for forecasts G14S and G14N starting at 1200 UTC 14 September 1988. For comparison, the observed minimum sea level pressure is also plotted.

particular, the observationally forced symmetric component from the initialization system may not have been sufficiently adapted to the model resolution, prohibiting the maintenance of the generated structure. In G25N, the storm underwent a gradual spinup as indicated by the decrease of minimum sea level pressure and increase of low-level winds that continued until the model storm made landfall after 66 h.

Finally, it is interesting to note that in all of the six forecasts of Hurricane Gloria, the southern portion of the eyewall of the model storm began to weaken as the model storm moved north, with no significant precipitation occurring south of the storm. As mentioned in KBTR, it appeared that this structure change was due primarily to the influence of the large-scale flow on the vortex and agrees with observed radar pictures of Hurricane Gloria during this time (Franklin et al. 1988).

d. Hurricane Gilbert (1200 UTC 14 September 1988)

The time series for integrations G14S and G14N are presented in Fig. 16. Since this experiment began just prior to landfall on the Yucatan Peninsula (Fig. 8), filling of the storm system in G14S began from the start of the experiment. The observed storm at the initial time was about 35 mb deeper than the storm in G14S, since the model resolution could not reproduce the extreme intensity of the storm. After emerging over the Gulf of Mexico, the storm in G14S underwent slow reintensification (less than 10 mb) until it approached the Mexican coast. The general behavior of the storm in G14S was in fairly good agreement with the observed storm, which reintensified very little as it moved over the waters of the Gulf of Mexico. The storm intensity in G14N was relatively constant (variation of about 5 mb) throughout the integration, with the storm weakening only slightly as it passed over the Yucatan Peninsula and gradually weakening again after crossing the Mexican coast.

5. Summary and concluding remarks

In this study the initialization scheme proposed by Kurihara et al. (1993) to specify the initial storm structure of tropical cyclones was tested on four real-data cases, using the GFDL triply nested movable mesh hurricane model. The error statistics for each of the four sets of forecasts are summarized in Table 5. Also included are the error statistics for the CLIPER model, based on climatology and persistence (Neumann and Pelissier 1981) and run from the best-track positions, and those for the NHC operational forecast made near the start of each integration. Use of the specified vortex produced a considerable improvement over both the CLIPER forecast as well as the NHC operational forecast for nearly every forecast period. Also, use of the specified vortex reduced the average 48-h forecast error by more than 50% when compared to the integrations run with the analyzed vortex. The reduction of forecast errors in the early period is especially important since these forecast times are a higher priority operationally

TABLE 5. Summary of the forecast error (km) for the four cases presented in this study. Included in each case are the two experiments with the GFDL hurricane model (with the analysis vortex and the specified vortex, respectively), CLIPER, and the NHC operational forecast.

Time	24 h	48 h	72 h
Gloria (1200 UTC 22 September 1985)			
Best-track CLIPER	140	280	494
NHC operational forecast	212	336	514
Analysis vortex	119	458	329
Specified vortex	56	206	274
Gloria (0000 UTC 24 September 1985)			
Best-track CLIPER	78	234	522
NHC operational forecast	102	198	398
Analysis vortex	137	173	132
Specified vortex	85	118	221
Gloria (0000 UTC 25 September 1985)			
Best-track CLIPER	154	317	—
NHC operational forecast	92	165	480
Analysis vortex	189	58	226
Specified vortex	47	30	259
Gilbert (1200 UTC 14 September 1988)			
Best-track CLIPER	157	387	828
NHC operational forecast	64	150	654
Analysis vortex	125	73	150
Specified vortex	44	22	109
Average			
Best-track CLIPER	132	305	615
NHC operational forecast	118	212	512
Analysis vortex	143	191	209
Specified vortex	58	94	216

due to their use in decisions regarding evacuation and civil defense. Much of this improvement resulted from the elimination of the erratic storm motion during the first 48 h of the uninitialized integrations, where the vortex resolved by the global analysis adjusted to the prediction model. Since the specified vortices were generated using an axisymmetric version of the hurricane model, they were well adapted to the model resolution and physics and, hence, very little adjustment occurred. After 48 h the difference in the track error between the two integrations generally decreased, with comparable 72-h average track errors. Most of the error during this later period appeared to be a result of errors in the forecasted evolution of the large-scale flow field and was affected very little by the use of the specified vortex. Thus, the primary impact of the specified vortex on the track prediction was to reduce the forecast error during the initial 36–48-h period. In some cases, however, the decrease of the forecast error during the early period of the forecast could result in significant improvements in the forecast of the storm track during the later period as well.

With a more accurately represented initial vortex structure the model successfully predicted changes in the storm intensity during various phases of the storm history. Since storm intensity is sensitive to the initial moisture field, the success of these intensity predictions was probably also due in part to the more realistic moisture field generated by the initialization scheme within the region of the specified vortex. In one case of Hurricane Gloria, which began before the onset of rapid intensification of the hurricane (G22S), the model correctly forecasted rapid intensification of the storm. The intensification leveled off at approximately the same time as observed, with gradual weakening during the final part of the forecast, in good agreement with the observed storm history. In another case of Hurricane Gloria, in which the forecast began during the period of rapid storm intensification (G24S), the initialized model storm continued to deepen from the beginning of the integration, without an initial adjustment or fluctuation in the storm intensity. However, neither integration reproduced the degree of very rapid deepening that occurred during this period, probably due to the model resolution that was still not able to resolve the very detailed structure in the eye and eyewall region. In the third forecast, which began as the hurricane reached its mature stage (G25S), the initialized model forecast maintained the storm intensity from the beginning, although some weakening occurred initially. However, the model failed to forecast the gradual weakening of the hurricane that began 12 h later. Finally, in the case of Hurricane Gilbert (G14S), after weakening as it moved over the Yucatan Peninsula, the model storm underwent moderate reintensification during the next 48 h as it moved over the Gulf of Mexico, similar to the observed storm system. In each of the four cases tested, the model was successful in correctly predicting changes in the storm intensity, at least to a first degree. For the predictions involving Hurricane Gloria, the intensity forecasts demonstrated improvements over the NHC operational forecasts for all three cases at 48 h and for two of the three cases at 72 h. In KBTR, the GFDL model had demonstrated skill for track prediction but not for intensity prediction. Therefore, the success of the intensity forecasts using the initialization scheme is dramatic evidence of the importance of an accurate initial vortex structure to correctly predict this quantity.

Where an accurate forecast of the storm track is made (e.g., G24S), the model has also demonstrated skill in accurately forecasting the magnitude and asymmetric distribution of the maximum low-level winds as verified with available observations. Successful prediction of this quantity was probably dependent on successful prediction of changes in both the storm structure and intensity that occurred as Hurricane Gloria approached the coast. The influences of the initialization scheme on the forecast of this quantity were twofold. First, the more realistic initial vortex structure resulted in a more accurate radius of maximum wind during the forecast period compared to the uninitialized storm. Second, while the vortex in the uninitialized forecast continued to intensify as the observed storm weakened, the storm winds in the forecast with the specified vortex gradually decreased as the storm continued moving north. We anticipate that our initialization scheme combined with a high-resolution operational model may yield useful forecasts of the low-level wind in many situations involving hurricanes and other tropical disturbances.

In the studies shown here a certain amount of subjectivity was used in determining some of the storm parameters (such as the filter radius r_o, the position of the vortex in the global analysis, or the length of the integration of the axisymmetric model). Also, the estimate of the tangential wind profile used in the scheme of vortex generation was determined from aircraft observations that are not typically available in real-time forecasting situations. However, as reported in section 6 of KBR, the entire initialization process has recently been automated to run from the type of datasets that are typically available in real-time situations. To determine the sensitivity to the implementation of the automated procedure outlined in KBR, all four cases were rerun using the automated procedure, with observational input from the marine advisories. This yielded average forecast errors of 51, 77, and 183 km at 24, 48, and 72 h in contrast to 58, 94, and 216 km for the integrations analyzed in this study. Thus, in the present experiments the impact of the automated procedure on the forecast of the storm motion was small. A study is under way on how to obtain the most benefit from aircraft data and other observations when they become available. In summary, given reasonable observations of the vortex structure these results suggest that the new initialization scheme shows promise in significantly improving the prediction of tropical cy-

clones. The entire initialization package has recently been tested on more real-data cases with continued satisfactory results. Some track errors for additional cases using the automated system have been included in Fig. 6 of KBR.

Acknowledgments. The authors would like to thank J. Mahlman for his continuous support of the Hurricane Dynamics Project at GFDL. They are also grateful to E. Kalnay, R. Kistler, and B. Katz of NMC for their cooperation in providing the data from the T80 analysis and for making integrations of their T80 forecast model that was used as the host model for the four sets of experiments presented in this study. Special thanks are also given to C. McAdie of NHC for supplying us with the CLIPER and NHC forecasts presented in this study. The authors are also grateful to W. Stern of GFDL for providing the programs used to convert the spectral data to gridpoint data. They would also like to express their appreciation to A. Broccoli and J. Sirutis of GFDL for their comments and criticisms on the original version of this manuscript, and to the reviewers, including Lloyd Shapiro, for their valuable comments. Finally, special thanks and credit are given to P. Tunison, C. Raphael, and J. Varanyak for preparing the figures.

APPENDIX A

Specification of Roughness and Evaporation Efficiency

The Matthews (1983) vegetation dataset provides a $1° \times 1°$ global specification of vegetation type (based on 32 vegetation categories), including the fractional area of cultivation within each 1° square. The vegetation type is used to specify horizontally varying values of surface roughness z_0 and evaporation efficiency W for use in the computation of the model surface fluxes. For model resolutions finer than 1°, the vegetation type of each fine-resolution grid square is set to the vegetation type of the 1° square in which it is contained. The values of z_0 for each vegetation type are computed from the formula $z_0 = 0.1(aH)$, where H is a typical height of a particular vegetation type and a is the fraction of the total height to which the wind can penetrate, that is, the correction factor due to the zero-plane displacement. The value of a is set to 1 for grassland, 4/5 for shrubland, and 2/3 for forest and woodland. Table A1 lists the values of z_0 for each vegetation type.

The evaporation efficiency W is assumed to be related to three factors: $W = w_1 w_2 w_3$. Here, w_1 is the ratio of potential evaporation of the most favorable

TABLE A1. Vegetation-related values of z_0 and w_2.

Vegetation type	Description	z_0 (m)	w_2
1	tropical evergreen rainforest, mangrove forest	3.33	1.0
2	tropical–subtropical evergreen seasonal broad-leaved forest	1.33	0.8
3	subtropical evergreen rainforest	2.00	0.9
4	temperate–subpolar evergreen rainforest	2.00	0.8
5	temperate evergreen seasonal broad-leaved forest, summer rain	1.33	0.7
6	evergreen broad-leaved sclerophyllous forest, winter rain	0.67	0.5
7	tropical–subtropical evergreen needle-leaved forest	2.00	0.8
8	temperate–subpolar evergreen needle-leaved forest	2.00	0.7
9	tropical–subtropical drought, deciduous forest	0.07	0.4
10	cold-deciduous forest, with evergreens	1.33	0.5
11	cold-deciduous forest, without evergreens	1.33	0.4
12	xeromorphic forest and woodland	0.33	0.4
13	evergreen broad-leaved sclerophyllous woodland	0.33	0.3
14	evergreen needle-leaved woodland	2.00	0.6
15	tropical–subtropical drought-deciduous woodland	2.00	0.3
16	cold-deciduous woodland	1.33	0.3
17	evergreen broad-leaved shrubland and thicket, dwarf-shrubland	0.40	0.4
18	evergreen needle-leaved or microphyllous shrubland	0.08	0.3
19	drought-deciduous shrubland and thicket	0.40	0.2
20	cold deciduous subalpine–subpolar or dwarf shrubland	0.08	0.2
21	xeromorphic shrubland–dwarf shrubland	0.08	0.1
22	arctic–alpine tundra, mossy bog	0.02	0.1
23	tall–medium–short grassland with 10%–40% tree cover	0.50	0.3
24	tall–medium–short grassland with less than 10% tree cover	0.05	0.2
25	tall–medium–short grassland with shrub cover	0.05	0.2
26	tall grassland, no woody cover	0.10	0.2
27	medium grassland, no woody cover	0.05	0.1
28	meadow, short grassland, no woody cover	0.05	0.1
29	forb formations	0.10	0.1
30	desert	0.01	0.01
31	ice	0.001	1.0
32	cultivation	0.20	0.4

land surface condition (i.e., rain forest) to the evaporation from the pure water surface. In the equatorial belt (10°N–10°S), the annual mean evaporation ratio between the land and ocean is 0.75 (Budyko 1956, Table 14) and, thus, w_1 is set to 0.8. The factor w_2, which ranges from 0 to 1, represents the long-term (climatic) water-availability condition. On the assumption that this condition is related to the height and type of plant foliage, the values of w_2 for each vegetation type are subjectively specified so that w_2 roughly corresponds to the inverse of the aridity index used in the geobotanical zonality graph (Budyko 1956). The specified values that are listed in Table 6 are largest for tropical rain forests and smallest for the desert-type vegetation. The final factor, w_3, indicates short-term soil moisture and plant conditions. It will be less than 1 when soil moisture is below a threshold value. At present, w_3 is set to 1, although it could be related to crop-moisture indices, for example.

APPENDIX B

Smoothing and Desmoothing

Previous versions of the hurricane model have included a simple three-point smoother applied sequentially in the zonal and meridional directions at appropriate time-step intervals to control grid-scale variation. This approach has the undesirable effect of also damping waves with longer wavelengths during removal of the short grid-scale variations. For example, sinusoidal waves of wavelength $4d$ or $6d$ (where d is the grid distance) are reduced in amplitude by 50% or 25% by the smoothing operator. This damping of longer wavelengths is now reduced through use of a "desmoothing" operator applied to the smoothed field. The above-mentioned $4d$ and $6d$ sinusoidal waves after desmoothing have amplitudes only 22% and 4% smaller than the original unsmoothed amplitudes.

The smoothing–desmoothing operator in the zonal direction is

$$L_Z(x) = (1 - 4\nu)X_0 + 2\nu(X_W + X_E) \quad \text{(B.1)}$$

and, similarly, in the meridional direction

$$L_M(x) = (1 - 4\nu)X_0 + 2\nu(X_N + X_S), \quad \text{(B.2)}$$

where X_0 is the center gridpoint value, X_i (i = W, E, N, or S) is the interface value between X_0 and its surrounding points, and ν is set to 0.25 for smoothing and −0.28 for desmoothing. All variables, except mixing ratio, are smoothed and then desmoothed. The fields of mixing ratio are smoothed but not desmoothed because negative mixing ratio values can be generated in some instances.

Additionally, the smoothing of the mass fields has been extended to land regions (previously this was omitted due to the complications of topography). Mass smoothing and desmoothing is now performed over land using an adjustment of the surface pressure p_s and temperature T from the height at the grid interfaces to the center gridpoint height. The interface values of X_i in the zonal and meridional operators of (B.1) and (B.2) are replaced by height-adjusted values:

$$p'_{s_i} = p_{s_i}\left[1 + \frac{\Gamma(z_{*,i} - z_{*,0})}{T_{\text{Kmax},i}}\right]^{g/R\Gamma} \quad \text{(B.3)}$$

and

$$T'_i = T_i + \Gamma(z_i - z_0), \quad \text{(B.4)}$$

where Γ is the standard lapse rate (6.7 K km^{-1}); $T_{\text{Kmax},i}$ is the near surface air temperature; z_* is the ground elevation; and z_0 is the height of the model sigma surface at the center grid point.

REFERENCES

Bender, M. A., R. E. Tuleya, and Y. Kurihara, 1987: A numerical study of the effect of island terrain on tropical cyclones. *Mon. Wea. Rev.*, **115**, 130–155.

Budyko, M. I., 1956: Heat balance of the earth's surface. Gidrometeorzdat, Leningrad, 255 pp. (English translation by N. A. Stepanova, Office of Technical Services, U.S. Dept. of Commerce, Washington, 1958.)

Carr, L. E., and R. L. Elsberry, 1990: Observational evidence for predictions of tropical cyclone propagation relative to environmental steering. *J. Atmos. Sci.*, **47**, 542–546.

Case, R. A., 1986: Atlantic hurricane season of 1985. *Mon. Wea. Rev.*, **114**, 1390–1405.

Franklin, J. L., S. J. Lord, and F. D. Marks, 1988: Dropwindsonde and radar observations of the eye of Hurricane Gloria (1985). *Mon. Wea. Rev.*, **116**, 1237–1244.

Kurihara, Y., 1973: A scheme of moist convective adjustment. *Mon. Wea. Rev.*, **101**, 547–553.

——, and R. E. Tuleya, 1974: Structure of a tropical cyclone developed in a three-dimensional numerical simulation model. *J. Atmos. Sci.*, **31**, 893–919.

——, and M. A. Bender, 1980: Use of a movable nested mesh model for tracking a small vortex. *Mon. Wea. Rev.*, **108**, 1792–1809.

——, C. L. Kerr, and M. A. Bender, 1989: An improved numerical scheme to treat the open lateral boundary of a regional model. *Mon. Wea. Rev.*, **117**, 2714–2722.

——, M. A. Bender, and R. J. Ross, 1993: An initialization scheme of hurricane models by vortex specification. *Mon. Wea. Rev.*, **121**, 2030–2045.

——, ——, R. E. Tuleya, and R. J. Ross, 1990: Prediction experiments of Hurricane Gloria, 1985, using a multiply-nested movable mesh model. *Mon. Wea. Rev.*, **118**, 2185–2198.

Matthews, E., 1983: Global vegetation and land use: New high-resolution data bases for climate studies. *J. Clim. Appl. Meteor.*, **22**, 474–487.

Mellor, G. L., and T. Yamada, 1974: A hierarchy of turbulence closure models for planetary boundary layers. *J. Atmos. Sci.*, **31**, 1791–1806.

Neumann, C. J., and J. M. Pelissier, 1981: Models for the prediction of tropical cyclone motion over the North Atlantic: An operational evaluation. *Mon. Wea. Rev.*, **109**, 522–538.

Orlanski, I., and J. J. Katzfey, 1987: Sensitivity of model simulations for a coastal cyclone. *Mon. Wea. Rev.*, **115**, 2792–2821.

Ross, R. J., and Y. Kurihara, 1992: A simplified scheme to simulate asymmetries due to the beta effect in barotropic vortices. *J. Atmos. Sci.*, **49**, 1620–1628.

Smith, R. K., W. Ulrich, and G. Dietachmayer, 1990: A numerical study of tropical cyclone motion using a barotropic model. Part 1: The role of vortex asymmetries. *Quart. J. Roy. Meteor. Soc.*, **116**, 337–362.

Tuleya, R. E., M. A. Bender, and Y. Kurihara, 1984: A simulation study of the landfall of tropical cyclones using a movable nested-grid model. *Mon. Wea. Rev.*, **112**, 124–136.

Wu, J., 1982: Wind-stress coefficients over sea surface from breeze to hurricane. *J. Geo. Res.*, **87**, 9704–9706.